

# Avoiding catastrophic failure in correlated network of networks

Saulo D. S. Reis<sup>1,2</sup>, Yanqing Hu<sup>1</sup>, Andrés Babino<sup>3</sup>, José S. Andrade Jr.<sup>2</sup>,

Santiago Canals<sup>4</sup>, Mariano Sigman<sup>3,5</sup>, Hernán A. Makse<sup>1,2,3</sup>

<sup>1</sup> *Levich Institute and Physics Department,*

*City College of New York, New York, New York 10031, USA*

<sup>2</sup> *Departamento de Física, Universidade Federal*

*do Ceará, 60451-970 Fortaleza, Ceará, Brazil*

<sup>3</sup> *Departamento de Física, FCEN-UBA,*

*Ciudad Universitaria, (1428) Buenos Aires, Argentina*

<sup>4</sup> *Instituto de Neurociencias, CSIC-UMH,*

*Campus de San Juan, Avenida Ramón y Cajal,*

*03550 San Juan de Alicante, Spain*

<sup>5</sup> *Universidad Torcuato Di Tella, Sáenz Valiente 1010,*

*C1428BIJ Buenos Aires, Argentina*

## Abstract

Networks in nature do not act in isolation but instead exchange information, and depend on each other to function properly [1–3]. An incipient theory of Networks of Networks have shown that connected random networks may very easily result in abrupt failures [3–6]. This theoretical finding bares an intrinsic paradox [8, 9]: If natural systems organize in interconnected networks, how can they be so stable? Here we provide a solution to this conundrum, showing that the stability of a system of networks relies on the relation between the internal structure of a network and its pattern of connections to other networks. Specifically, we demonstrate that if network inter-connections are provided by hubs of the network and if there is a moderate degree of convergence of inter-network connection the systems of network are stable and robust to failure. We test this theoretical prediction in two independent experiments of functional brain networks (in task- and resting states) which show that brain networks are connected with a topology that maximizes stability according to the theory.

Over the last decade the science of complex networks has flourished, describing the organization of a myriad of natural systems including societies, Internet, the brain and cell organization, as a web of interacting nodes [7]. This research program demonstrated that many critical properties of a system organization, growth and robustness, depend on how nodes are interconnected and are relatively independent of the specific identity of each node.

More recently, this argument has been pushed further. Nodes organize into networks, but these emergent systems do not occur in isolation from other networks. Instead, more often networks exchange information, and depend on each other to function properly [3–6]. A paradigmatic example is the power and communication networks [1–3, 6]: communication network nodes rely for power supply on the power stations and, reciprocally, the power stations function properly exchanging information through the communication network. Understanding how stability and information flow are affected by these inter-dependencies constitutes a major challenge to understand the resilience of natural systems.

The theory of networks of networks has been built relying mainly on unstructured patterns of between-networks connectivity, namely with one-to-one random interconnections between dependent nodes [3, 6]. When two stable networks are fully interconnected with one-to-one random connections where every single node in a network depends on a node in the other network chosen at random, the interaction results in abrupt failures [3, 6]: small perturbations in one network are amplified on an interconnected network, which causes further damage to the originally perturbed network. This process leads to cascading failures which are argued to underlay catastrophic outcomes in man-made infrastructures such as blackouts in power grids [2, 3]. However, this theoretical finding bares an intrinsic paradox [8, 9]: If living systems— such as the brain [10] and cellular networks [11]— organize in interconnected networks, how can they be so stable?

Our conjecture is that the solution to this conundrum relies on the relation between the internal structure of the set of networks and its pattern of connections to other networks. Random networks are very efficient mathematical constructs to develop theory but the majority of networks observed in nature are correlated [12, 13]. Correlations, in turn, provide structure to the network. Indeed, the importance of degree correlations on the dynamical and structural properties of interconnected networks has been recently addressed in Ref. [14].

Most natural networks form hubs which make certain nodes of greater relevance. This

structure adds a degree of freedom to the system of networks by setting whether hubs of the network should be the nodes broadcasting information to other networks, or, conversely, whether across networks communication should be governed by nodes with less pertinence within the network.

We develop a full theory for systems of structured networks which identifies a structural communication protocol which assures that the system of networks is stable (less likely to break into catastrophic failures) and optimized for fast communication across the entire system. The theory establishes concrete predictions of a regime of correlated connectivity between networks composing the system.

We test these predictions with two different systems of brain connectivity based on functional magnetic resonance imaging (fMRI) data. The brain organizes in a series of interacting networks [10, 15] presenting a paradigmatic case study for a theory of connected correlated networks. We show that for two independent experiments of functional networks in task and resting state in humans, the systems of brain networks organize optimally as predicted by the theory.

Our results hence provide a plausible explanation to *(i)* the conundrum of why systems of networks were theoretically expected to show frequent catastrophic failure but this was not observed in nature, *(ii)* provide a specific theoretical prediction on how structured networks should be interconnected to be stable, and *(iii)* demonstrate in two examples of functional brain connectivity that the structure of across network connections lies in the range where the theory predicts stability for different functional architectures.

We present a theory based on a recursive set of equations to study the cascading failure and percolation process for two correlated interconnected networks. The theory is a generalization of the analytical approach for single networks of Moore and Newman [16] to study cascading behavior in interconnected correlated networks (analytic details in SI Section I). Here we refer to the most important aspects of the theory and the corresponding set of predictions. The theory can be extended to n-interconnected networks following Ref. [17].

We consider two interconnected networks, each one has a power-law degree distribution characterized by exponent  $\gamma$ ,  $P(k_{\text{in}}) \sim k_{\text{in}}^{-\gamma}$ , valid up to a cut-off  $k_{\text{max}}$  imposed by their finite size. Here  $k_{\text{in}}$  is the number of links of a node towards nodes in the same network. This implies that a few nodes will be vastly connected within the network (hubs) while the majority of nodes will be weakly connected to other nodes in the network.

The structure between interconnected networks can be characterized by two parameters:  $\alpha$  and  $\beta$  (Fig. 1a). The parameter  $\alpha$ , defined as

$$k_{\text{out}} \sim k_{\text{in}}^{\alpha}, \quad (1)$$

where  $k_{\text{out}}$  is the degree of a node towards nodes in the other network, determines the likelihood that hubs of each network are also the principal nodes connecting both networks. For  $\alpha > 0$  the nodes in network  $A$  and  $B$  which connect both networks will typically be hubs in  $A$  and  $B$  respectively (Fig. 1a, right panels). Instead, for  $\alpha < 0$  the two networks will be connected preferentially by nodes of low degree within each network (Fig. 1a, left panels).

The parameter  $\beta$  defines the indegree-indegree internetwork correlations as [12, 13]:

$$k_{\text{in}}^{\text{nn}} \sim k_{\text{in}}^{\beta}, \quad (2)$$

where  $k_{\text{in}}^{\text{nn}}$  is the average in-degree of the nearest-neighbors of a node in the other network. It determines the convergence of connections between networks, i.e. the likelihood that a link connecting networks  $A$  and  $B$  coincides in the same type of node. Intuitively, Eqs. (1)-(2) can be seen as a compromise between redundancy and reach of connections between both networks. For  $\beta > 0$  connections between networks are convergent (assortative, Fig. 1a, top panels), while for  $\beta < 0$  they are divergent (dissortative, Fig. 1a, bottom panels). Uncorrelated networks have  $\alpha = 0$  and  $\beta = 0$ .

We analyze how the system of two correlated networks breaks down after random failure (random attack) of a fraction  $1 - p$  nodes for different patterns of between-networks connectivity characterized by  $(\alpha, \beta)$ . We adopt the conventional percolation criterion of stability and connectivity measuring how the largest connected component breaks-down following the attack [3]. In classic percolation of single networks, two nodes of a network are randomly linked with probability  $p$  [18]. For low  $p$ , the network is fragmented into subextensive components. Percolation theory of random networks demonstrates that as  $p$  increases, there is a critical phase transition in which a single extensive cluster or giant component spans the system (the critical  $p$  is referred to as  $p_c$ ).

A robust notion of stability in a system of networks can be obtained by identifying  $p_c$  at which a cohesive mutually connected network breaks down into disjoint sub-components under different forms of attack. Network topologies with low  $p_c$  are robust, since this indicates that the majority of nodes ought to be removed to break it down. On the contrary,

high values of  $p_c$  are indicative of a fragile network which breaks down by only removing a few nodes.

Here we analyze two qualitatively different manners in which the networks interact and propagate failure. In one mode (*conditional interaction*, Fig. 1b) a node in network  $B$  cannot function (and hence is removed) if it loses all connectivity with network  $A$  after the attack [3]. In the second condition (*redundant interaction*, Fig. 1c) a node in network  $B$  may survive even if it is completely decoupled from network  $A$ , if it remains attached to the largest component of network  $B$  [4]. To understand why these two responses to failure are pertinent in real networks it helps to exemplify the interaction between power and data networks. If electricity can only flow through the cables of the power network, a node in the data network unplugged from the power system shuts off and stops functioning. This situation corresponds to two networks coupled in a conditional manner; a case treated in Ref. [3] considering one-to-one random connections between networks. Consider instead the case of a printer or any peripheral which can be plugged to the main electricity network but can also receive power through a USB cable by the computer. A node may still function even if it is disconnected from the other network, if it remains connected to its local network. This corresponds to the redundant interaction as treated by Ref. [4] in the unstructured case.

We first investigate the stability of two interacting scale-free networks for a value of  $\gamma$  set arbitrarily to 2.5 and  $k_{\max} = 100$  in a regime where each isolated network is stable and robust to attack [19]. The attack starts with the removal of a fraction of  $1 - p$  nodes chosen at random from both networks. This attack produces extra failures of, for instance, nodes in  $B$ , if (i) *conditional interaction*: they disconnect from the giant component of network  $A$  or disconnect from the giant component of  $B$ , or (ii) *redundant interaction*: they disconnect from the giant component of network  $A$  and the giant component of network  $B$ . In conditional mode, this process may lead to new failures in network  $A$  producing a cascade if they lose connectivity in  $B$ . Other nodes in  $A$  may also fail as they get disconnected from the giant component in  $A$ , and the cascading process iterates until converging to a final configuration. By definition, only the conditional mode may produce cascading effects but not the redundant mode. The theoretical analysis of this process leads to a set of recursive equations (SI Section I) that provides a stability phase diagram for the critical percolation threshold  $p_c(\alpha, \beta)$  under attack in redundant and conditional failures for a given  $(\gamma, k_{\max})$

as seen in Fig. 2.

Figure 2 reveals that the relation between a network internal structure and the pattern of connection between networks critically determines whether attacks lead to catastrophic cascading failures (high  $p_c$ ) or not (low  $p_c$ ). For conditional interactions, the system of networks is stable when  $\alpha < 0$  (indicated by low  $p_c(\alpha, \beta)$ , left-blue region in Fig. 2a) or for  $\alpha \gtrsim 0.5$  and  $\beta > 0$  (light blue top-right quadrant), and becomes particularly unstable for intermediate values of  $0 < \alpha < 0.5$  and  $\beta < 0$ . This result shows that the system of networks is stable when the hubs are protected  $\alpha < 0$  by being isolated from network-network connectivity or when, on the contrary, the bulk of connectivity within and across networks is sustained exclusively by a very small set of hubs (large  $\alpha, \beta$ ). Intermediate configurations where hubs interconnect with low-degree nodes, are highly unstable since hubs can be easily attacked via conditional interactions, and lead to catastrophic cascading after attack. Similar unstable configurations appear in the one-to-one random interconnectivity [3].

When two networks interact in a redundant manner, the system of networks is less vulnerable to attacks (Fig. 2b). This expected result is manifested by the fact that even for small values of  $p \sim 0.1$ , the system of networks remains largely connected for any  $(\alpha, \beta)$ . The non-intuitive observation is that the relation between a network internal structure and the pattern of connection between networks which optimizes stability differs from the conditional interaction (Fig. 2a). In fact,  $\alpha < 0$  leads to the less stable configurations (larger value of  $p_c$  in Fig. 2b, red region), and the only region which maximizes stability corresponds to high values of  $\alpha$  and  $\beta > 0$  (blue region in Fig. 2b), i.e. an interaction where connection between networks is highly redundant and carried only by a few hubs of each network. Thus, the parameters that maximize stability for both interactions lie in the region  $\alpha \approx 1$  and  $\beta > 0$ .

Systems of brain networks present an ideal candidate to examine this theory for the following reasons: (i) Local-brain networks organize according to a power-law degree distribution [20, 21], and (ii) some aspects of local function are independent of long-range global interactions with other networks (as in the redundant interaction) like the processing of distinct sensory features, while other aspects of local connectivity can be shut-down when connectivity to other networks is shut-down (as in conditional interaction) like integrative perceptual processing [22]. Hence, the theory predicts that to assure stability for both modes of dependencies, brain networks ought to be connected with positive and high values of  $\alpha$  and positive values of  $\beta$ .

In the next section we examine this hypothesis for two independent functional magnetic resonance imaging (fMRI) experiments: human-resting state data obtained from NYU public repository [23] and human dual-task data [24] previously used to investigate brain network topology [15, 25, 26] (see Methods Section and SI Section II for details). We first identify functional networks (in resting state, Fig. 3a and dual task, Fig. 3b) made of nodes connected by strong links, ie, by highly correlated fMRI signals [15]. These networks are interconnected by weak links (low-correlation in the fMRI signal) following the clustering methods of Ref. [15]. The indegree distribution of the system of networks follows a bounded power-law (Fig. 3c-d and Table I) and the exponents  $\alpha$  and  $\beta$  show high positive values for both experiments (Fig. 3e-f and Table I).

To examine whether these values are optimal for the specific  $(\gamma, k_{\max})$ -parameters of these networks, we projected for each experiment, the measured values of  $\alpha$  and  $\beta$  to the theoretically constructed stability phase diagram quantified by  $p_c(\alpha, \beta)$  in conditional and redundant mode (Fig. 4). Remarkably, the experimental values of  $\alpha$  and  $\beta$  (white circles) lie within the relatively narrow region of parameter space that minimizes failure for conditional and redundant interaction. Overall these results demonstrate that brain networks tested under distinct mental states share the topological features that confer stability to the system.

Our result hence provides a theoretical revision to the current view that systems of networks are highly unstable. We show that for structured networks, if the inter-connections are provided by hubs of the network ( $\alpha > 0.5$ ) and for moderate degrees of convergence of inter-network connection ( $\beta > 0$ ) the systems of network are stable. This stability holds in the conditional interaction [3] and in a more robust topology of redundant interaction [4]. The redundant condition is equivalent to stating that the system of networks merges in a single network (in-going and out-going links are treated as the same). Hence the condition of optimality for this topology equates to saying that the size of the giant component formed by the connection of both networks is optimized. As a consequence, the maximization of robustness for both conditions is equivalent to maximize *(i)* robustness in the more conventional conditional interaction, where links of one network are strictly necessary for proper function of the other network, and *(ii)* a notion of information flow and storage using classic percolation theory definition of the size of the maximal mutual component across both networks. In other words, these parameters form a set of interacting nodes which are maximally large in size and robust to failure.

The most natural metaphor for man-made system of networks is for electricity (wires) and the Internet or voice connectivity (data). A more direct analogue to this case in a living system such as the brain would be the interaction between anatomic, metabolic and vascular networks (wires) and their coupling to functional correlations (data) [27]. Here instead we adopted the theory of network of networks to investigate the optimality of coupled functional brain modules. The consistency between experimental data and theoretical predictions even in this broaden notion of coupled networks is suggestive of the possible broad scope of the theory making it a candidate to study a wider range of inter-connected networks [28].



## METHODS

**Experimental analysis.** The interdependent functional brain networks are constructed from fMRI data following the methods of Ref. [15]. First, the Blood Oxygen Level Dependent (BOLD) signal from each brain voxel (node) is used to construct the functional network topology based on standard methods [20, 21] using the equal-time cross-correlation matrix,  $C_{ij}$ , of the activity of pairs of voxels (see SI Section II).

The derivation of a binary graph from a continuous connectivity matrix relies on a threshold  $T$  where the links between two nodes (voxels)  $i$  and  $j$  are occupied if  $T < C_{ij}$  [15, 20] such as in bond percolation. A natural and non-arbitrary choice of threshold can be derived from a clustering bond percolation process. The size of the largest connected component of voxels as a function of  $T$  reveals clear percolation-like transitions [15] in the two datasets identified by the jumps in the size of the largest component in Fig. 3a-b. The emergent networks in resting state correspond to the medial prefrontal cortex, posterior cingulate, and lateral temporoparietal regions, all of them part of the default mode network (DMN) typically seen in resting state data [23]. In dual-task, as expected for an experiment involving visual and auditory stimuli and bi-manual responses, the responsive regions include bilateral visual occipito-temporal cortices, bilateral auditory cortices, motor, premotor and cerebellar cortices, and a large-scale bilateral parieto-frontal structure.

**Scaling of correlations in the brain.** We identify functional networks (see Fig. 3a-b right panels) made of nodes connected by strong links (strong BOLD signal correlation  $C_{ij}$ ) which are interconnected by weak links (weak BOLD signal correlation) [15, 29]. Statistical analysis based on standard maximum likelihood and KS methods [30] (see SI Section II A) yield the values of the indegree exponents of each functional brain network:  $\gamma = 2.85 \pm 0.04$  and  $k_{\max} = 133$  for resting state and  $\gamma = 2.25 \pm 0.07$ ,  $k_{\max} = 139$  for dual-task (Fig. 3c-d). The obtained exponent  $\alpha$  shows high positive values for both experiments:  $\alpha = 1.02 \pm 0.02$  and  $0.92 \pm 0.02$  for resting state and dual task data, respectively (Fig. 3e). The inter-network connections show positive exponents for both systems:  $\beta = 0.66 \pm 0.03$  and  $\beta = 0.79 \pm 0.04$  for resting state and dual-task, respectively (Fig. 3f).

Hence, in accordance with the predictions of the theory, these two interdependent brain networks derived from qualitatively distinct mental states (resting states and strong engagement in a task which actively coordinates visual, auditory and motor function) show consistently high values of  $\alpha$  and positive values of  $\beta$ . Figure 4 shows the theoretical phase

diagram  $p_c(\alpha, \beta)$  in conditional and redundant mode calculated for coupled networks with the experimental values  $\gamma = 2.25$  and  $2.85$ . Left panels show the prediction of  $p_c(\alpha, \beta)$  in the conditional mode of failure and right panels correspond to the redundant mode. The experimental  $(\alpha, \beta)$  are shown in white circles lying in stable regions of the phase diagram (low  $p_c$ ). Interestingly, the convergence of inter-network connections,  $\beta$ , is slightly higher under task conditions, adding a new degree of freedom to the system of networks, the dynamic allocation of functional connections governed by context-dependent processes such as attention or learning for the case of brain networks. Further research is assured to investigate the neuronal mechanisms underlying inter-network communication routines specified by  $\beta$ .

- 
- [1] Little, R. G. Controlling cascading failure: Understanding the vulnerabilities of interconnected infrastructures. *J. Urban Technology* **9**, 109-123 (2002).
- [2] Rosato, V. Modeling interdependent infrastructures using interacting dynamical models. *Int. J. Critical Infrast.* **4**, 63-79 (2008).
- [3] Buldyrev, S. V., Parshani, R., Paul, G., Stanley, H. E. & Havlin, S. Catastrophic cascade of failures in interdependent networks. *Nature* **464**, 1025-1028 (2010).
- [4] Leicht, E. A. & D'Souza, R. M. Percolation on interacting networks. Preprint available at <http://arxiv.org/abs/0907.0894> (2009).
- [5] Brummitt, C. D., D'Souza, R. M. & Leicht, E. A. Suppressing cascades of load in interdependent networks. *Proc. Natl. Acad. Sci. USA* **109**, E680-E689 (2012).
- [6] Gao, J., Buldyrev, S. V., Stanley, H. E. & Havlin, S. Networks formed from interdependent networks. *Nature Phys.* **8**, 40-48 (2012).
- [7] Dorogovtsev, S. N. *Lectures on Complex Networks* (Oxford Univ. Press, Oxford, 2010).
- [8] Bianconi, G., Dorogovtsev, S. N. & Mendes, J. F. F. Mutually connected component of network of networks. Preprint available at arXiv:1402.0215 (2014).
- [9] Bianconi, G. & Dorogovtsev, S. N. Multiple percolation transitions in a configuration model of network of networks. *Phys.Rev. E* **89**, 062814 (2014).
- [10] Dosenbach, N. U. F., *et al.* Distinct brain networks for adaptive and stable task control in humans. *Proc. Natl. Acad. Sci. USA* **104**, 11073-11078 (2007).
- [11] Vidal, M., Cusick, M. E. & Barabási, A.-L. Interactome networks and human disease. *Cell* **144**, 986-998 (2011).
- [12] Pastor-Satorras, R., Vázquez, A. & Vespignani, A. Dynamical and correlation properties of the Internet. *Phys. Rev. Lett.* **87**, 258701 (2001).
- [13] Gallos, L. K., Song, C. & Makse, H. A. Scaling of degree correlations and its influence on diffusion in scale-free networks. *Phys. Rev. Lett.* **100**, 248701 (2008).
- [14] Radicchi, F. Driving interconnected networks to supercriticality. *Phys. Rev. X* **4**, 021014 (2014).
- [15] Gallos, L. K., Makse, H. A. & Sigman, M. A small world of weak ties provides optimal global integration of self-similar modules in functional brain networks. *Proc. Natl. Acad. Sci. USA*

- 109**, 2825-2830 (2012).
- [16] Moore, C. & Newman, M. E. J. Exact solution of site and bond percolation on small-world networks. *Phys. Rev. E* **62**, 7059-7064 (2000).
  - [17] Gao, J., Buldyrev, S. V., Havlin, S. & Stanley, H. E. Robustness of a network formed by  $n$  interdependent networks with a one-to-one correspondence of dependent nodes. *Phys. Rev. E* **85**, 066134 (2012).
  - [18] Bollobás, B. *Random Graphs* (Academic Press, London, 1985).
  - [19] Cohen, R., Ben-Avraham, D. & Havlin, S. Percolation critical exponents in scale-free networks. *Phys. Rev. E* **66**, 036113 (2002).
  - [20] Eguiluz, V. M., Chialvo, D. R., Cecchi, G. A., Baliki, M. & Apkarian, A. V. Scale-free brain functional networks. *Phys. Rev. Lett.* **94**, 018102 (2005).
  - [21] Bullmore E. & Sporns O. Complex brain networks: graph theoretical analysis of structural and functional systems. *Nature Reviews Neuroscience* **10**, 186-198 (2009).
  - [22] Sigman, M., Pan, H., Yang, Y. H., Stern, E., Silbersweig, D. & Gilbert, C. D. Top-down reorganization of activity in the visual pathway after learning a shape identification task. *Neuron* **46**, 823-835 (2005).
  - [23] Shehzad, Z., Kelly, A. M. C. & Reiss, P. T. The resting brain: unconstrained yet reliable. *Cereb. Cortex* **10**, 2209-2229 (2009).
  - [24] Sigman, M. & Dehaene, S. Brain mechanisms of serial and parallel processing during dual-task performance. *J. Neurosci.* **28**, 7585-7598 (2008).
  - [25] Russo, R., Herrmann, H. J. & de Arcangelis, L. Brain modularity controls the critical behavior of spontaneous activity. *Sci. Rep.* **4**, 4312 (2014).
  - [26] Gallos, L. K., Sigman, M. & Makse, H. A. The conundrum of functional brain networks small-world efficiency or fractal modularity. *Front. Physiol.* **3**, 123 (2012).
  - [27] Honey, C. J., Sporns, O., Cammoun, L., Gigandet, X., Thiran, J. P., Meuli, R. & Hagmann, P. Predicting human resting-state functional connectivity from structural connectivity. *Proc. Natl. Acad. Sci. USA* **106**, 2035-2040 (2009).
  - [28] Schneider, C. M., Yazdani, N., Araújo, N. A. M., Havlin, S. & Herrmann, H. J. Towards designing robust coupled networks. *Sci. Rep.* **3**, 1969 (2013).
  - [29] Schneidman, E., Berry, M. J., Segev, R. & Bialek, W. Weak pairwise correlations imply strongly correlated network states in a neural population. *Nature* **440**, 1007-1012 (2006).

- [30] Clauset, A., Shalizi, C. R. & Newman, M. E. J. Power-law distributions in empirical data. *SIAM Rev.* **51**, 661-703 (2009).

### **Acknowledgements**

This work was funded by NSF-PoLS PHY-1305476 and NIH-NIGMS 1R21GM107641. We thank N. A. M. Araújo, S. Havlin, L. Parra, L. Gallos, A. Salles and T. Bekinschtein for clarifying discussions. Additional financial support was provided by CNPq, CAPES, FUNCAP, the Spanish MINECO BFU2012-39958, CONICET and the James McDonnell Foundation 21st Century Science Initiative in Understanding Human Cognition - Scholar Award.

### **Author contributions**

All authors contributed equally to the work presented in this paper.

### **Additional information**

The authors declare no competing financial interests. Supplementary information accompanies this paper on [www.nature.com/naturephysics](http://www.nature.com/naturephysics). Reprints and permissions information is available online at <http://npg.nature.com/reprintsandpermissions>. Correspondence and requests for materials should be addressed to H.A.M.

**FIG. 1. Modeling degree-degree correlations between interconnected networks.**

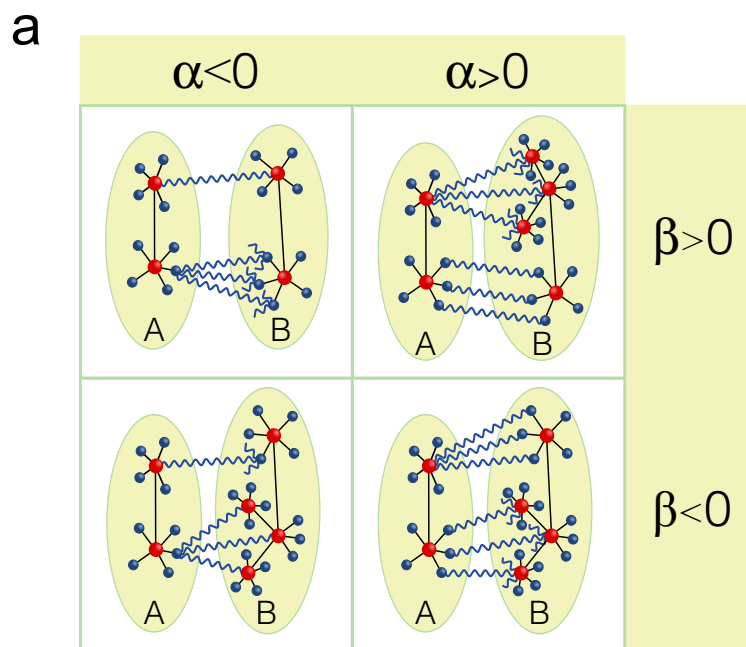
**a**, Hubs (red nodes) and non-hubs (blue nodes) have  $k_{\text{out}}$  outgoing links (wiggly blue links) according to the parameter  $\alpha$ . When  $\alpha < 0$ , the outgoing links are more likely to be found attached to non-hub nodes. When  $\alpha > 0$ , hubs are favored over non-hub nodes. Nodes from different networks are connected according to  $\beta$ . When  $\beta > 0$ , nodes with similar degree prefer to connect between themselves, and when  $\beta < 0$ , nodes connect dissasortatively. For simplicity we exemplify the outgoing links emanating from only a few nodes in network  $A$  according to  $(\alpha, \beta)$ . **b**, Conditional mode of failure: a node fails every time it becomes disconnected from the largest component of its own network, or loses all its outgoing links. All stable nodes have at least one out-going link. We exemplified only one cascading path for simplicity. In reality, we investigate the cascading produced by removal of  $1 - p$  nodes from both networks. With the failure of the hub indicated in the figure (Stage 1), all its non-hub neighbors also fail because they become isolated from the giant component in  $A$  (Stage 2). In Stage 3 the upper hub from network  $B$  fails, due to the conditional interaction, since it loses connectivity with network  $A$  even though it is still connected in  $B$ . With the failure of this second hub all its non-hub neighbors become isolated, leading to their failure (Stage 4). This leads to a further removal of the second outgoing link and the cascading failure propagates back to network  $A$  (Stage 5). Since no more nodes become isolated, the cascading failure stops with the mutual giant component shown in Stage 5. At this point we measure the fraction of nodes in the giant component of  $A$  and  $B$ . **c**, Redundant interaction: The failure of a node only leads to further failure if its removal isolates its neighbors in the same network. The failure of the hub (Stage 1) do not propagate the damage to the other network (Stage 2 and 3) and therefore there is no cascading in this interaction. We measure the fraction of nodes in the mutually connected giant component. We note that nodes can be stable even if they do not have out-going links as long as they belong to the mutually connected component. Thus, the mutually connected giant component may contain nodes which are not part of the single giant component of one of the networks as shown in Stage 3, network  $A$ .

**FIG. 2. Stability phase diagram of  $p_c(\alpha, \beta)$  for conditional and redundant failure.** Percolation threshold  $p_c(\alpha, \beta)$  predicted by theory for coupled networks for generic values  $\gamma = 2.5$  and  $k_{\text{max}} = 100$  in **a**, conditional interaction and **b**, redundant interaction. We use a bounded power-law for closer comparison with experimental data. For a given sys-

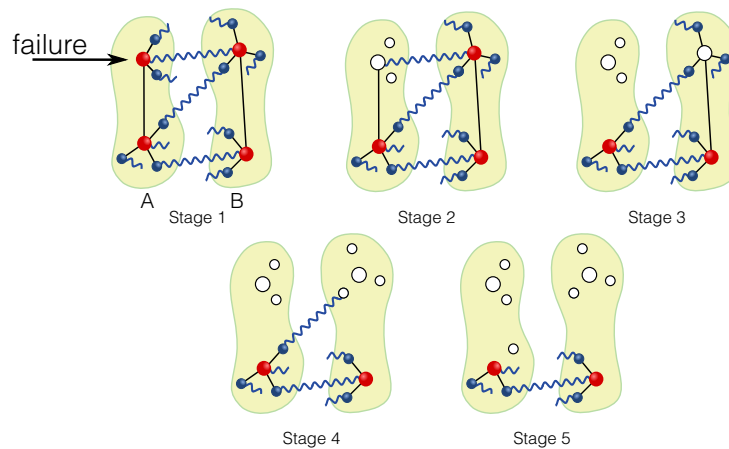
tem, the results are independent of the cut-off. For the conditional interaction the system is more stable (low value of  $p_c$ ) when  $\alpha < 0$  as well as for  $\alpha \approx 1$  and  $\beta > 0$ , and displays a maximum in  $p_c$  (unstable) around  $\alpha \approx 0.25$  and  $\beta < 0$ . The redundant interaction instead is most unstable for  $\alpha < 0$  and becomes stable for  $\alpha \approx 1$  and  $\beta > 0$ . Thus the best compromise between both modes of failures is for values located in the upper-right quadrant  $\alpha \approx 1$ ,  $\beta > 0$ .

**FIG. 3. Analysis of interconnected functional brain networks.** **a**, Clustering analysis to obtain the system of networks for resting state data for a typical subject out of 12 scans analyzed. Left plot shows the fraction of nodes in the largest network versus  $T$ . We identify one percolation-like transition with the jump at  $T_c = 0.854$ . Strong in-going links define the networks and correspond to  $T > T_c$  [15]. At  $T_c$ , the two largest networks, shown in the right panel in the network representation and in the inset in the brain, merge. Interconnecting weak out-going links are defined for  $0.781 < T < T_c$  (plotted in grey). **b**, The same clustering analysis is done to identify the interconnected network in dual task [15]. We show a typical scan out of a total of 16 subjects. The strong ingoing links have  $T > T_c = 0.914$ , and weak outgoing links  $0.864 < T < T_c$ . **c**, The in-degree  $k_{\text{in}}$  distribution for the resting state and **d**, dual task experiment. **e**, Out-degree  $k_{\text{out}}$  as a function of  $k_{\text{in}}$  for resting state and dual task, according to Eq. (1). **f**,  $k_{\text{in}}^{\text{nn}}$  as a function of  $k_{\text{in}}$  for resting state and dual task experiments, according to Eq. (2).

**FIG. 4. Stability phase diagram for brain networks.** Percolation threshold  $p_c(\alpha, \beta)$  obtained from theory for two coupled networks with power-law exponents and cutoff given by the brain networks in **a**, resting state and **b**, dual task. The left panels are for conditional interactions and the right panels for redundant interactions. The white circles represent the data points of the real brain networks. They indicate that the brain structure results from a compromise of optimal stability between both modes of failure.



**b Conditional interaction**



**c Redundant interaction**

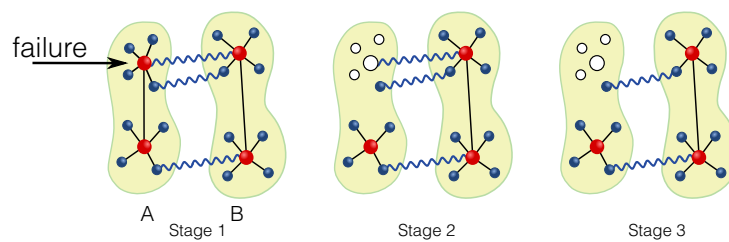


FIG. 1.



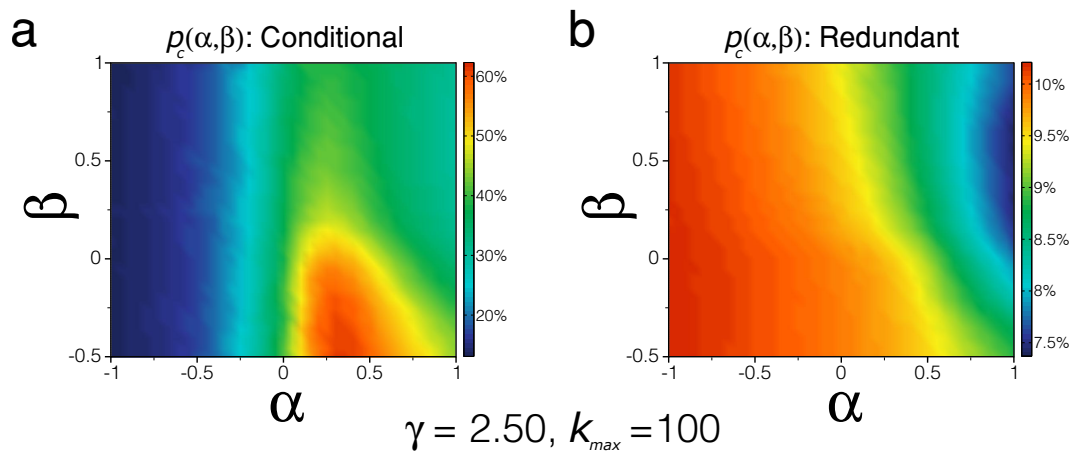


FIG. 2.

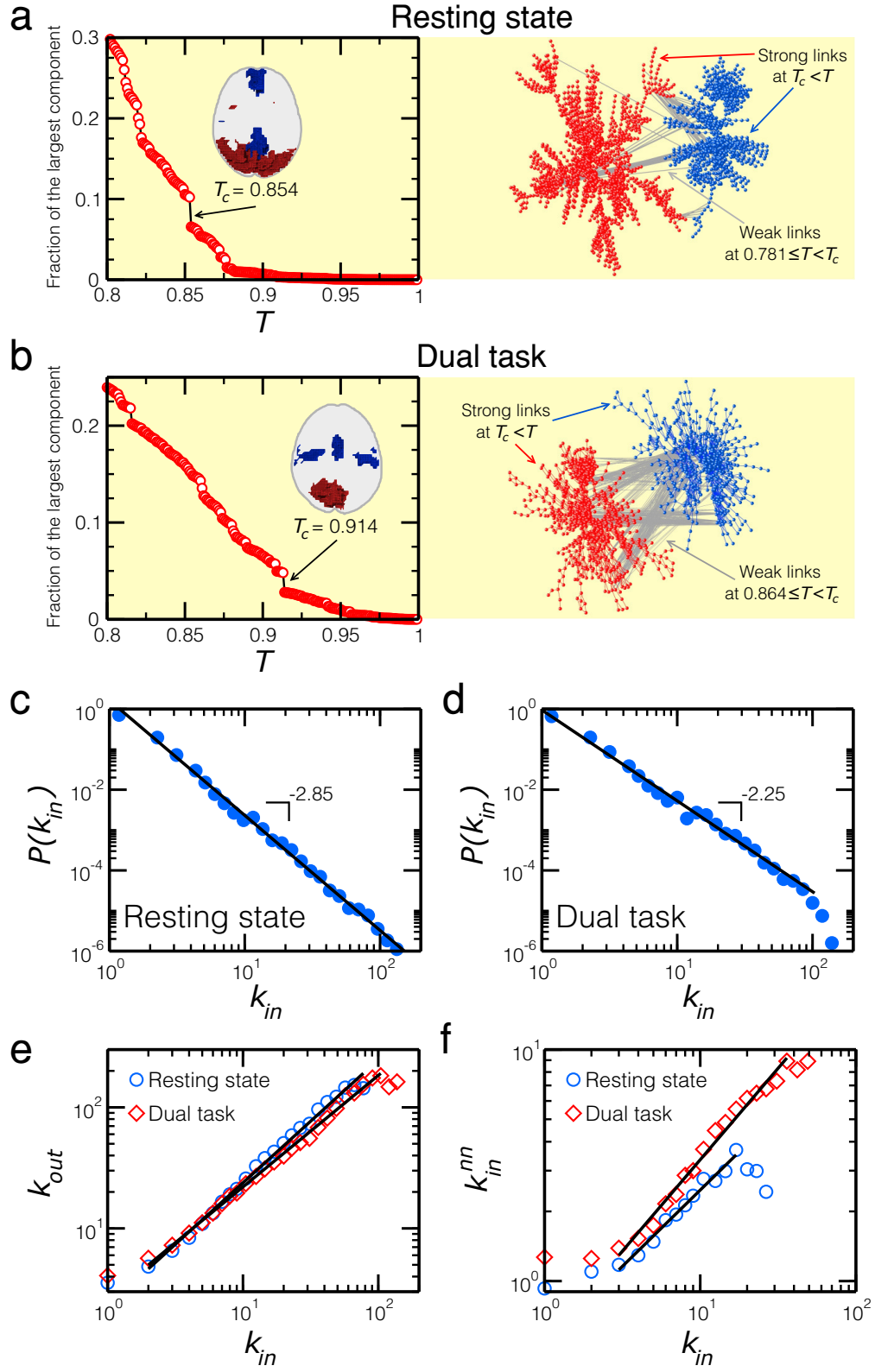


FIG. 3.

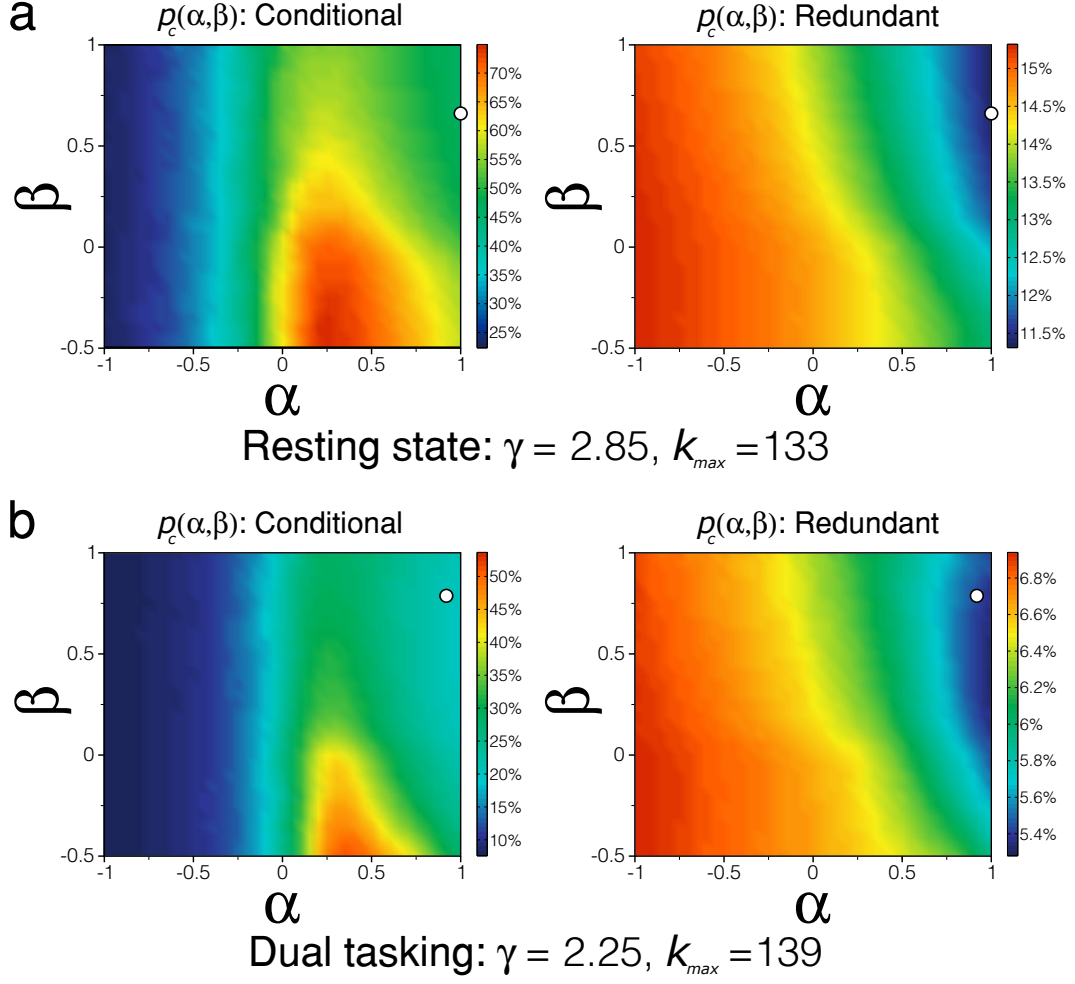


FIG. 4.

Dataset	$\gamma$	$\alpha$	$\beta$	$k_{\max}$
Human Resting State	$2.85 \pm 0.04$	$1.02 \pm 0.02$	$0.66 \pm 0.03$	133
Human Dual Task	$2.25 \pm 0.07$	$0.92 \pm 0.02$	$0.79 \pm 0.04$	139

TABLE I. Parameters characterizing the studied human brain networks.

## SUPPLEMENTARY INFORMATION

### Avoiding catastrophic failure in correlated network of networks

Reis, Hu, Babino, Andrade, Canals, Sigman, Makse

#### I. THEORY OF CORRELATED NETWORK OF NETWORKS

We first illustrate the theory to calculate the percolation threshold for a single uncorrelated network following the standard calculations done by Moore and Newman [16]. We then generalize this theory to the case of two correlated interconnected networks to calculate  $p_c$  under redundant and conditional modes of failures.

##### A. Calculation of percolation threshold for a single network [16]

The percolation problem of a single network can be solved by the calculation of the probability  $X$  to reach the giant component by following a randomly chosen link [16]. First, choose a link of a single network at random. After that, select one of its ends with equal probability. The probability  $1 - X$  is the probability that, by following this link using the chosen direction, we do not arrive at the giant component, but instead we connect to a finite component.

Since the degree distribution of an end node of a chosen link is given by  $kP(k)/\langle k \rangle$ , one can write down a recursive equation for  $X$  as:

$$X = 1 - \sum_k \frac{kP(k)}{\langle k \rangle} (1 - X)^{k-1}. \quad (3)$$

The sum is for the probability that, by following the chosen link, we arrive at a node with degree  $k$  which is not attached to the giant component through its remaining  $k - 1$  connections. We rewrite the previous equation as follows:

$$X = 1 - \sum_k \frac{kP(k)}{\langle k \rangle} \mathcal{G}(X), \quad (4)$$

where

$$\mathcal{G}(X) = (1 - X)^{k-1}. \quad (5)$$

Once the probability  $X$  is known, we can use it to write the probability  $1 - S$  that a randomly chosen node does not belong to the giant component. Again, this is a sum of

probabilities: the probability that this node has no links attached to it, plus the probability that this node has one link and this link does not lead to the giant component, plus the probability that this node has two links and none of them leads to the giant component, and so on. In other words:

$$1 - S = \sum_k P(k)(1 - X)^k. \quad (6)$$

Again, we can rewrite this equation as:

$$S = 1 - \sum_k P(k)\mathcal{H}(X), \quad (7)$$

where

$$\mathcal{H}(X) = (1 - X)^k. \quad (8)$$

Note that the probability  $S$  not only stands for the probability of choosing one node from the giant component at random, but also provides the fraction of nodes in the network occupied by the giant component. Equation (7) provides the probability of a node to belong to the giant component and is the main quantity to be calculated by the theory from where the value of the percolation threshold can be calculated as the largest value of  $p_c$  such that  $S(p_c) = 0$ .

## B. Analytical approach for two interconnected networks with correlations

Now, we present a generalization of the above approach suited to both problems studied in our work, namely, the redundant and conditional interactions of two interconnected networks with generic correlations. We have also developed an analogous theoretical framework based on the generating approach used in Ref. [3]. However, we find that the generating function approach [3] is more mathematically cumbersome if one wants to take into account the correlations between the networks to calculate the mutually connected giant component. Since the size of the giant component is the only quantity needed in this study, we find that the approach of Moore and Newman is more transparent and, furthermore, allows us to take into account both modes of failure in a single theory. Indeed, the whole theory can be cast into a few number of equations, while the generating function approach is more involved.

We define two probabilities for network  $A$  (and their equivalents for network  $B$ ). As we did for the case of a single network, we will take advantage of functions similar to  $\mathcal{G}(X)$  and

$\mathcal{H}(X)$ . By doing this, the following recursive equations are general and can be applied to the redundant and to the conditional interaction cases depending of the way the functions  $\mathcal{G}(\bullet)$  and  $\mathcal{H}(\bullet)$  are written for each case. Therefore, below we develop the theory for both modes of failure and later we specialize on each interaction.

First, we define the probability  $X_A$ , as the probability that, by following a randomly chosen link of network  $A$ , we reach a node from the largest connected component of network  $A$ . The second probability,  $Y_{k_{\text{in}}^A}$ , is the probability of choosing at random a node from network  $A$  with in-degree  $k_{\text{in}}^A$  connected with a node from the largest component of network  $B$ . Analogously, we define probabilities  $X_B$  and  $Y_{k_{\text{in}}^B}$  for network  $B$ .

Thus, if we initially remove a fraction  $1 - p_A$  of nodes from network  $A$  chosen at random, and a fraction  $1 - p_B$  of nodes from network  $B$ , we can write  $X_A$  and  $X_B$  in analogy with Eq. (4) [we note that when network  $A$  and network  $B$  have the same number of nodes,  $p = (p_A + p_B)/2$ ]:

$$X_A = p_A \left[ 1 - \sum_{k_{\text{in}}^A, k_{\text{out}}^A} \frac{k_{\text{in}}^A P(k_{\text{in}}^A, k_{\text{out}}^A)}{\langle k_{\text{in}}^A \rangle} \mathcal{G}(X_A, Y_{k_{\text{in}}^A}, k_{\text{in}}^A, k_{\text{out}}^A) \right]. \quad (9)$$

Here, the correlations between  $k_{\text{in}}^A$  and  $k_{\text{out}}^A$  from Eq. (1) are quantified by  $P(k_{\text{in}}^A, k_{\text{out}}^A)$ , which is the joint probability distribution of in- and out-degrees of nodes from network  $A$  from where Eq. (1) can be derived. The probability function  $\mathcal{G}(X_A, Y_{k_{\text{in}}^A}, k_{\text{in}}^A, k_{\text{out}}^A)$  in Eq. (9) is analogous to Eq. (5). It stands for the probability that, by following a randomly chosen link from network  $A$ , we reach a node which is not part of the giant component of network  $A$ , which has in-degree  $k_{\text{in}}^A$  and out-degree  $k_{\text{out}}^A$  and/or is not connected with a node from the giant component network  $B$  (here and in what follows, “and/or” refers to the nature of the two cases of study: the redundant and conditional interactions, respectively). To write down Eq. (9) we use the joint in- and out-degree distribution of an end node of a randomly chosen in-link  $k_{\text{in}}^A P(k_{\text{in}}^A, k_{\text{out}}^A) / \langle k_{\text{in}}^A \rangle$ . Finally, the terms in the squared brackets stand for the probability  $X_A = X_A(p_A = 1)$  before removing the fraction  $1 - p_A$ , which is the generalization of Eq. (4). Thus, after the removal of a fraction  $1 - p_A$ , the probability of following a randomly selected in-link to reach a node which belongs to the giant cluster of  $A$  is  $X_A(p_A = 1)$  times the probability  $p_A$  for this node being a survival node. In a similar fashion, we write the probability  $X_B$ , the joint degree distribution  $P(k_{\text{in}}^B, k_{\text{out}}^B)$  and the probability function  $\mathcal{G}(X_B, Y_{k_{\text{in}}^B}, k_{\text{in}}^B, k_{\text{out}}^B)$  for network  $B$ :

$$X_B = p_B \left[ 1 - \sum_{k_{\text{in}}^B, k_{\text{out}}^B} \frac{k_{\text{in}}^B P(k_{\text{in}}^B, k_{\text{out}}^B)}{\langle k_{\text{in}}^B \rangle} \mathcal{G}(X_B, Y_{k_{\text{in}}^B}, k_{\text{in}}^B, k_{\text{out}}^B) \right]. \quad (10)$$

For the probability  $Y_{k_{\text{in}}^A}$  of choosing at random a node from the network  $A$  with degree  $k_{\text{in}}^A$  connected through an out-link with a node from the giant component of  $B$ , we write down the following expression:

$$Y_{k_{\text{in}}^A} = p_B \left[ 1 - \sum_{k_{\text{in}}^B} P(k_{\text{in}}^B | k_{\text{in}}^A) (1 - X_B)^{k_{\text{in}}^B} \right]. \quad (11)$$

The term inside the squared brackets is the probability of choosing a node from network  $B$  which is not part of the giant component of  $B$  and it is connected with a node from network  $A$  of in-degree  $k_{\text{in}}^A$ . Naturally,  $Y_{k_{\text{in}}^A}$  is this probability times the probability  $p_B$  of the  $B$ -node being a survival node after the removal of a fraction  $1 - p_B$  of nodes from network  $B$ . To write down this equation, we use the conditional probability  $P(k_{\text{in}}^B | k_{\text{in}}^A)$  of a node from network  $B$  with in-degree  $k_{\text{in}}^B$  being connected with a node with in-degree  $k_{\text{in}}^A$  from network  $A$ , and the probability that, by following an in-link from  $B$ , we do not reach the giant component of  $B$ ,  $(1 - X_B)$ . The conditional probability  $P(k_{\text{in}}^B | k_{\text{in}}^A)$  quantify the correlations expressed by Eq. (2). Similar equation can be written for  $Y_{k_{\text{in}}^B}$ :

$$Y_{k_{\text{in}}^B} = p_A \left[ 1 - \sum_{k_{\text{in}}^A} P(k_{\text{in}}^A | k_{\text{in}}^B) (1 - X_A)^{k_{\text{in}}^A} \right]. \quad (12)$$

With  $X_A$ ,  $X_B$ ,  $Y_{k_{\text{in}}^A}$ , and  $Y_{k_{\text{in}}^B}$  on hand, it is possible to compute the fraction of survival nodes in the giant component of network  $A$ ,  $S_A$ , and in network  $B$ ,  $S_B$ , through the relations analogous to Eq. (7):

$$S_A = p_A \left[ 1 - \sum_{k_{\text{in}}^A, k_{\text{out}}^A} P(k_{\text{in}}^A, k_{\text{out}}^A) \mathcal{H}(X_A, Y_{k_{\text{in}}^A}, k_{\text{in}}^A, k_{\text{out}}^A) \right], \quad (13)$$

and

$$S_B = p_B \left[ 1 - \sum_{k_{\text{in}}^B, k_{\text{out}}^B} P(k_{\text{in}}^B, k_{\text{out}}^B) \mathcal{H}(X_B, Y_{k_{\text{in}}^B}, k_{\text{in}}^B, k_{\text{out}}^B) \right]. \quad (14)$$

The probability function  $\mathcal{H}(X_A, Y_{k_{\text{in}}^A}, k_{\text{in}}^A, k_{\text{out}}^A)$  generalizes Eq. (8), and stands for the probability of randomly selecting a node from network  $A$  with in-degree  $k_{\text{in}}^A$  and out-degree  $k_{\text{out}}^A$ , which is not in the giant component of  $A$  and/or it is not connected with the giant

component of  $B$  (again, and/or refers to redundant and conditional modes of interaction, respectively).

Due to the different meanings that the probability function  $\mathcal{H}(X_A, Y_{k_{\text{in}}^B}, k_{\text{in}}^A, k_{\text{out}}^A)$  may assume depending of the mode of interaction, for this general approach the nature of the quantities  $S_A$  and  $S_B$  differ conceptually from the quantity  $S$  presented by Eq. (7) for a single network. See Fig. 5 for more details. For the conditional mode, a node, or a set of nodes from network  $A$ , for example, will fail if (i) it loses connection with the largest component of network  $A$ , or if (ii) it loses connection with the largest component of network  $B$ . Thus  $\mathcal{H}(X_A, Y_{k_{\text{in}}^B}, k_{\text{in}}^A, k_{\text{out}}^A)$  is the probability function that describes the probability of picking a node at random from network  $A$  that is not part of the largest component of  $A$  (due to condition (i) this node will fail) **or** that is not connected to the largest cluster of network  $B$  (due to condition (ii) this node will also fail). Thus,  $S_A$  (and its counterpart  $S_B$  for network  $B$ ) is the fraction occupied by the largest component of survival node in network  $A$ . For a finite size network,  $S_A = n_A/N_A$ , where  $n_A$  is the number of nodes in the largest component and  $N_A$  the number of nodes in network  $A$ . It is important to note that due to the condition (ii) this fraction is necessarily the same as the size of the giant connected component of network  $A$ .  $S_A$  may be interpreted also as the fraction from network  $A$  that is part of the mutually connected giant component  $S_{AB}$ , as in Ref. [3]. The same applies to network  $B$ . In other words, the number of nodes in the mutually connected giant component belonging to  $B$  is the same as the number of nodes in the giant connected component of  $B$  as calculated after the attack as if  $B$  was a single network.

For the redundant mode, since there is no cascading propagation of damage due to the failure of a neighbor,  $\mathcal{H}(X_A, Y_{k_{\text{in}}^B}, k_{\text{in}}^A, k_{\text{out}}^A)$  is the function that describes the probability of picking a node at random, for example from network  $A$ , which is not connected to the largest component from its own network, network  $A$ , **and** is not connected to the largest component of network  $B$  via an out-going link. Therefore, the quantity  $S_A$  provides the fraction of “active” nodes, or in other words, the fraction of survival nodes that may be part of the largest component of network  $A$ , and in addition a fraction from network  $A$  that are disconnected from that largest component of network  $A$ , but are not failed because they are still connected to the largest component of network  $B$  via an out-going link. Thus, the mutually connected giant component  $S_{AB}$  has a different structure in this mode compared to the conditional mode. This situation is illustrated in Fig. 1c and 5. At the end of the



attack process, there is a remaining node in network  $A$  which is not connected to the giant component of  $A$  calculated as if it is a single network. Such a node is still “on” since it is connected to  $B$  via an out-going link. Thus, the mutually connected giant component contains this node.

Furthermore, a node that has lost all its out-going link will fail in the conditional interaction, even if it is still connected to its own giant component. However, in the redundant mode, a node without out-going links may still function as long as it is still connected to the giant component of its own single network. For instance, many nodes are still functioning in Fig. 1c, redundant mode, even though they are not interconnected. However, in conditional interaction Fig. 1b, all stable nodes need to have out-going links. That is, in redundant mode, the nodes can still receive power via the same network or the other network, while in the conditional node, they need out-going connectivity all the time. Taking into account these considerations, the value of  $p_c$  is obtained from the behavior of the giant component of either of the networks in the conditional mode, while in the redundant mode, the value of  $p_c$  is obtained from the size of the mutually giant connected component. However, in this last case, it is statistically the same to obtain  $p_c$  from the giant components of one of the networks as well. In what follows the calculations of the giant components are done by considering two networks of equal size  $N$  and damaging each network with a fraction  $1 - p$  of nodes.

Next, we explicitly write the probability functions  $\mathcal{G}$  and  $\mathcal{H}$  for both, conditional and redundant interactions, respectively, to occur on interactive networks after a random failure of  $1 - p_A$  and  $1 - p_B$  nodes. It is important to note that the probabilities  $\mathcal{G}$  and  $\mathcal{H}$  describe the probability of randomly choosing a node which is not part of the giant component of one network and/or is not connected to a node from the giant component of the adjacent network. In other words, this node picked at random is not part of the giant component of the whole network. We test the general case where both networks are attacked:  $p_A \neq 1$  and  $p_B \neq 1$ . The theory can be used to attacking only one network by setting  $p_B = 1$ .

**Redundant interaction:** We consider the total fraction  $1 - p$  of nodes removed from the two networks. If network  $A$  and network  $B$  have the same number of nodes, then  $p = (p_A + p_B)/2$ . For redundant interaction two events are important. Both events are defined as follows. The first is the probability that, by following a randomly chosen link of a network, we do not reach the giant component of that network. For network  $A$ , this

probability can be written as  $(1 - X_A)$ . The second is the probability of choosing at random a node from one network, say network  $A$ , with in-degree  $k_{\text{in}}^A$  which is not connected with a node from the giant component of network  $B$ . This probability can be written as  $(1 - Y_{k_{\text{in}}^A})$ . In the case of redundant interaction (with no cascading due to conditional mode) these two probabilities are independent, since the lack of connectivity with network  $B$  does not imply failure of a node from network  $A$ . Thus, the probability function  $\mathcal{G}(X_A, Y_{k_{\text{in}}^A}, k_{\text{in}}^A, k_{\text{out}}^A)$  that, by following a randomly selected link we arrive at a node with in-degree  $k_{\text{in}}^A$  and out-degree  $k_{\text{out}}^A$  which is not part of the giant cluster of its own network and is not connected with a node from the giant cluster of the adjacent network can be written as:

$$\mathcal{G}(X_A, Y_{k_{\text{in}}^A}, k_{\text{in}}^A, k_{\text{out}}^A) = (1 - X_A)^{k_{\text{in}}^A - 1} (1 - Y_{k_{\text{in}}^A})^{k_{\text{out}}^A}. \quad (15)$$

Similarly, the probability function  $\mathcal{H}(X_A, Y_{k_{\text{in}}^A}, k_{\text{in}}^A, k_{\text{out}}^A)$  of picking a node, at random, with in-degree  $k_{\text{in}}^A$  and out-degree  $k_{\text{out}}^A$  from one network which is not part of the giant cluster of its own network and is not connected with a node from the giant cluster from the adjacent network is:

$$\mathcal{H}(X_A, Y_{k_{\text{in}}^A}, k_{\text{in}}^A, k_{\text{out}}^A) = (1 - X_A)^{k_{\text{in}}^A} (1 - Y_{k_{\text{in}}^A})^{k_{\text{out}}^A}. \quad (16)$$

Again, we can write equivalent expressions for  $\mathcal{G}(X_B, Y_{k_{\text{in}}^B}, k_{\text{in}}^B, k_{\text{out}}^B)$  and  $\mathcal{H}(X_B, Y_{k_{\text{in}}^B}, k_{\text{in}}^B, k_{\text{out}}^B)$  as

$$\mathcal{G}(X_B, Y_{k_{\text{in}}^B}, k_{\text{in}}^B, k_{\text{out}}^B) = (1 - X_B)^{k_{\text{in}}^B - 1} (1 - Y_{k_{\text{in}}^B})^{k_{\text{out}}^B}, \quad (17)$$

and

$$\mathcal{H}(X_B, Y_{k_{\text{in}}^B}, k_{\text{in}}^B, k_{\text{out}}^B) = (1 - X_B)^{k_{\text{in}}^B} (1 - Y_{k_{\text{in}}^B})^{k_{\text{out}}^B}. \quad (18)$$

**Conditional interaction:** This interaction leads to cascading processes. In the conditional interaction process, we are interested in the cascading effects on the coupled networks,  $A$  and  $B$ , due to an initial random failure of a portion of nodes in both networks, where  $p_A \neq 1$  and  $p_B \neq 1$ . In the case of attacking network  $A$  only, the fraction  $p_B$  is set to be equal to one, such that a node from network  $B$  can only fail due to the conditional interaction.

For the conditional interaction,  $\mathcal{G}(X_A, Y_{k_{\text{in}}^A}, k_{\text{in}}^A, k_{\text{out}}^A)$  depends on the probability that, by following a link from network  $A$ , we do not arrive at a node with in-degree  $k_{\text{in}}$  connected to the giant component of its own network,  $(1 - X_A)^{k_{\text{in}} - 1}$ , and on the probability of randomly choosing a node from network  $A$  with  $k_{\text{out}}$  outgoing links towards network  $B$ ,  $(1 - Y_{k_{\text{in}}^A})^{k_{\text{out}}}$ . Also, we have the probability  $\mathcal{H}(X_A, Y_{k_{\text{in}}^A}, k_{\text{in}}^A, k_{\text{out}}^A)$  of picking up a node from one network

which is not part of the giant component of its own network or picking up one node from one network which is not connected with one node from the giant component of the adjacent network, which is also dependent of the probabilities  $(1 - X_A)$  and  $(1 - Y_{k_{\text{in}}^A})$ .

Different from the redundant mode, these probabilities,  $(1 - X_A)$  and  $(1 - Y_{k_{\text{in}}^A})$ , are not mutually exclusive in the conditional interaction. Thus:

$$\mathcal{G}(X_A, Y_{k_{\text{in}}^A}, k_{\text{in}}^A, k_{\text{out}}^A) = (1 - X_A)^{k_{\text{in}}^A - 1} + (1 - Y_{k_{\text{in}}^A})^{k_{\text{out}}^A} - (1 - X_A)^{k_{\text{in}}^A - 1} (1 - Y_{k_{\text{in}}^A})^{k_{\text{out}}^A}, \quad (19)$$

and

$$\mathcal{H}(X_A, Y_{k_{\text{in}}^A}, k_{\text{in}}^A, k_{\text{out}}^A) = (1 - X_A)^{k_{\text{in}}^A} + (1 - Y_{k_{\text{in}}^A})^{k_{\text{out}}^A} - (1 - X_A)^{k_{\text{in}}^A} (1 - Y_{k_{\text{in}}^A})^{k_{\text{out}}^A}. \quad (20)$$

We can write the equivalent expressions for  $\mathcal{G}(X_B, Y_{k_{\text{in}}^B}, k_{\text{in}}^B, k_{\text{out}}^B)$  and  $\mathcal{H}(X_B, Y_{k_{\text{in}}^B}, k_{\text{in}}^B, k_{\text{out}}^B)$  as follows:

$$\mathcal{G}(X_B, Y_{k_{\text{in}}^B}, k_{\text{in}}^B, k_{\text{out}}^B) = (1 - X_B)^{k_{\text{in}}^B - 1} + (1 - Y_{k_{\text{in}}^B})^{k_{\text{out}}^B} - (1 - X_B)^{k_{\text{in}}^B - 1} (1 - Y_{k_{\text{in}}^B})^{k_{\text{out}}^B}, \quad (21)$$

and

$$\mathcal{H}(X_B, Y_{k_{\text{in}}^B}, k_{\text{in}}^B, k_{\text{out}}^B) = (1 - X_B)^{k_{\text{in}}^B} + (1 - Y_{k_{\text{in}}^B})^{k_{\text{out}}^B} - (1 - X_B)^{k_{\text{in}}^B} (1 - Y_{k_{\text{in}}^B})^{k_{\text{out}}^B}. \quad (22)$$

With the set of equations (15)-(16) and (19)-(20), and their equivalents for network  $B$ , Eq. (17)-(18) and (21)-(22), it is possible to solve both problems, the redundant and the conditional interactions, on a system of two coupled networks interconnected through degree-degree correlated outgoing nodes. The correlation between the coupled networks is represented by the in- out-degree distribution  $P(k_{\text{in}}^A, k_{\text{out}}^A)$  and by the conditional probability  $P(k_{\text{in}}^B | k_{\text{in}}^A)$ . In the following section, we present the network model used to generate a system of two networks interconnected with correlations described by power law functions with the exponents  $\alpha$  and  $\beta$ . These networks are used on the calculations of the distribution  $P(k_{\text{in}}^A, k_{\text{out}}^A)$  and  $P(k_{\text{in}}^B | k_{\text{in}}^A)$  for each pair of  $(\alpha, \beta)$ . The final result is the probability for a node to belong to the giant component of network  $A$  or  $B$ — as given by Eq. (13) and (14)— as a function of the fraction of removed nodes  $1 - p$  (with  $p_A = p_B = p$ ) from where the percolation threshold  $p_c$  can be evaluated from  $S_A(p_c) = 0$  and  $S_B(p_c) = 0$  as a function of the three exponents defining the networks:  $\gamma$ ,  $\alpha$  and  $\beta$ , and the cutoff in the degree distribution  $k_{\text{max}}$ . We use two networks of equal size  $N = 1500$  nodes, each.

### C. Network model. Test of theory

In order to test the percolation theory using the above formalism, we need to generate a system of interacting networks with the prescribed set of exponents and degree cutoff. The first step of our network model is to generate two networks,  $A$  and  $B$ , with the same number  $N$  of nodes and with the desired in-degree distribution  $P(k_{\text{in}})$  as defined by  $\gamma$  and the maximum degree  $k_{\text{max}}$ . To do this we use the standard “configuration model” which has been extensively used to generate different network topologies with arbitrary degree distribution [7]. The algorithm of the configuration model basically consists of assigning a randomly chosen degree sequence to the  $N$  nodes of the networks in such a way that this sequence is distributed as  $P(k_{\text{in}}) \sim k_{\text{in}}^{-\gamma}$  with  $1 \leq k_{\text{in}} \leq k_{\text{max}}$  and  $P(k_{\text{in}}) = 0$  for  $k_{\text{in}} > k_{\text{max}}$ . After that, we select a pair of nodes at random, both with  $k_{\text{in}} > 0$ , and we connect them.

The next step of the model is to connect networks  $A$  and  $B$  in such a way that their outgoing nodes have degree-degree correlations that can be described by the parameters  $\alpha$  and  $\beta$  as defined in Eqs. (1) and (2). In order to do this, we use an algorithm inspired by the configuration model. First, we assign a sequence of out-degrees  $k_{\text{out}}$  to the nodes of each network. This process is performed independently to each network by adding the same number of outgoing links. Each outgoing link is added individually to nodes chosen at random with a probability that is proportional to  $k_{\text{in}}^\alpha$ . Thus, an out-degree sequence is assigned to the nodes in each network in such a way that  $k_{\text{out}} \sim k_{\text{in}}^\alpha$  according to Eq. (1). This process results in a set of outgoing stubs attached to every node in network  $A$  and  $B$ . The next step is to join these stubs in such a way that we satisfy the correlations given by Eq. (2).

The next step is to choose two nodes, one from each network, such that  $\langle k_{\text{in}}^{\text{nn}} \rangle = A \times k_{\text{in}}^\beta$ , and then, we connect them if they have available outgoing links. Here, we choose the factor  $A$  such that  $\langle k_{\text{in}}^{\text{nn}} \rangle = 1$  for  $k_{\text{in}} = 1$  when  $\beta = 1$ , and  $\langle k_{\text{in}}^{\text{nn}} \rangle = k_{\text{max}}$  for  $k_{\text{in}} = 1$  and  $\beta = -1$ . Thus, we write the value of the factor as  $A = A(k_{\text{max}}, \beta) = k_{\text{max}}^{(1-\beta)/2}$ .

The algorithm works as follows: we randomly choose one node  $i$  from one network. After that, we choose another node  $j$ , from the second network, with in-degree  $k_{\text{in}}^j$  with probability that follows a Poisson distribution  $P(k_{\text{in}}^j, \lambda)$ , where the mean value  $\lambda = \langle k_{\text{in}}^{\text{nn}} \rangle$ . We connect nodes  $i$  and  $j$  if they are not connected yet.

It should be noted that Eqs. (1) and (2) may not be self-consistent for all values of

$\alpha, \beta$ . For instance, for very low values of  $\beta$ , e.g.,  $\beta = -1$ , the degree correlations between coupled networks are not always self-consistent with the structural relations between  $k_{\text{in}}$  and  $k_{\text{out}}$  described by  $\alpha$ . Since  $\beta$  measures the convergence of connections between networks, when  $\beta$  is negative hubs prefer to connect with low-degree nodes. To better understand these features, consider  $\beta = -1$ , and for nodes with  $k_{\text{in}} = 1$  and  $k_{\text{in}} = k_{\text{max}}$ . With this configuration, nodes with  $k_{\text{in}} = 1$  are likely to be connected with nodes from the adjacent network with  $k_{\text{in}} = k_{\text{max}}$ . When  $\alpha = 1$ , most of the links are attached to the highly active nodes, notably, nodes with  $k_{\text{in}} = k_{\text{max}}$ , and less likely to nodes with  $k_{\text{in}} = 1$ . In this regime, there are not enough low-degree nodes with outgoing links to be connected with the high-degree nodes, thus the desired relation between  $k_{\text{in}}^{\text{nn}}$  versus  $k_{\text{in}}$  cannot be realized. The other possible situation is when  $\alpha$  is negative. In this regime, most of the outgoing links are attached to low-degree nodes, consequently, the few hubs from the network are unlikely to receive an outgoing link, and even when it happens, one hub does not have enough outgoing links to be connected to the stubs of the low-degree nodes. For these reasons we limit our study to  $\alpha > -1$  and  $\beta > -0.5$  where the relations are found to be self-consistent.

For every initial pair  $(\alpha, \beta)$ , we generate a network with the above algorithm and then we recalculate the effective values of  $(\alpha, \beta)$  which are then used to plot the phase diagram  $p_c(\alpha, \beta)$  in Fig. 2 and 4.

#### D. Calculation of the giant components and percolation threshold $p_c(\gamma, \alpha, \beta, k_{\text{max}})$

With the networks generated in the previous section we are able to compute the functions  $P(k_{\text{in}}^{\text{A}}, k_{\text{out}}^{\text{A}})$  and  $P(k_{\text{in}}^{\text{B}}|k_{\text{in}}^{\text{A}})$ . Then we apply the recursive equations derived previously to calculate the size of the giant components  $S_{\text{A}}$  and  $S_{\text{B}}$  from Eqs. (13) and (14). We do this calculation for different values of  $p$  for cases of study and then extract the percolation threshold  $p_c$  at which the giant components  $S_{\text{A}}$  and  $S_{\text{B}}$  vanish in conditional mode.

Figure 6 shows the predictions of the theory in the conditional mode for a network with  $\gamma = 2.5$ ,  $\alpha = 0.5$ ,  $\beta = 0.5$  and  $k_{\text{max}} = 100$ . We plot the relative size of the giant components in  $A$  and  $B$ ,  $S_{\text{A}}$  and  $S_{\text{B}}$ , as predicted by Eqs. (13) and (14). As one can see in Fig. 6, there is a well-defined critical value at which the  $A$ -giant component vanishes which defines the percolation threshold  $p_c(\gamma, \alpha, \beta, k_{\text{max}}) = 0.335$  for these particular parameters.

Figure 6 also presents the comparison between theoretical results and direct simulations.

We test the theory by attacking randomly the generated correlated networks and calculating numerically the giant components versus the fraction of removed nodes  $1 - p$ . The results show a good agreement corroborating the theory.

After testing the theory, a full analysis is done spanning a large parameter space by changing the four parameters defining the theory:  $(\gamma, \alpha, \beta, k_{\max})$ . The results are plotted in the main text Fig. 2 and 4 for the stated values of the parameters. Beyond the calculation of  $p_c(\alpha, \beta)$ , we also identify regimes of first-order phase transitions in the conditional interaction, found specially when  $p_c$  is high, beyond the standard second-order percolation transition; a result that will be expanded in subsequent papers.

## II. EXPERIMENTS: ANALYSIS OF INTERCONNECTED BRAIN NETWORKS

Our functional brain networks are based on functional magnetic resonance imaging (fMRI). The fMRI data consists of temporal series, known as the blood oxygen level-dependent (BOLD) signals, from different brain regions. The brain regions are represented by voxels. In this work we use data sets gathered in two different and independent experiments. The first is the NYU public data set from resting state humans participants. The NYU CSC TestRetest resource is available at [http://www.nitrc.org/projects/nyu\\_trt/](http://www.nitrc.org/projects/nyu_trt/). The second data set was gathered in a dual-task experiment on humans previously produced by our group [24] and recently analyzed in Ref. [15]. The brain networks analyzed here can be found at: [http://lev.ccny.cuny.edu/~hmakse/soft\\_data.html](http://lev.ccny.cuny.edu/~hmakse/soft_data.html). Both datasets were collected in healthy volunteers and using 3.0T MRI systems equipped with echoplanar imaging (EPI). The first study was approved by the institutional review boards of the New York University School of Medicine and New York University. The second study is part of a larger neuroimaging research program headed by Denis Le Bihan and approved by the Comité Consultatif pour la Protection des Personnes dans la Recherche Biomédicale, Hôpital de Bicêtre (Le Kremlin-Bicêtre, France).

**Resting state experiments:** A total of 12 right-handed participants were included (8 women and 4 men, mean age 27, ranging from 21 to 49). During the scan, participants were instructed to rest with their eyes open while the word Relax was centrally projected in white, against a black background. A total of 197 brain volumes were acquired. For fMRI a gradient echo (GE) EPI was used with the following parameters: repetition time

(TR) = 2.0 s; echo time (TE) = 25 ms; angle = 90°; field of view (FOV) = 192 × 192 mm; matrix = 64 × 64; 39 slices 3 mm thick. For spatial normalization and localization, a high-resolution T1-weighted anatomical image was also acquired using a magnetization prepared gradient echo sequence (MP-RAGE, TR = 2500 ms; TE = 4.35 ms; inversion time (TI) = 900 ms; flip angle = 8°; FOV = 256 mm; 176 slices). Data were processed using both AFNI (version AFNI\_2011.12.21.1014, <http://afni.nimh.nih.gov/afni>) and FSL (version 5.0, [www.fmrib.ox.ac.uk](http://www.fmrib.ox.ac.uk)) and the help of the [www.nitrc.org/projects/fcon\\_1000](http://www.nitrc.org/projects/fcon_1000) batch scripts for preprocessing. The preprocessing consisted on: motion correcting (AFNI) using Fourier interpolation, spatial smoothing (fsl) with gaussian kernel (FWHM=6mm), mean intensity normalization (fsl), FFT band-pass filtering (AFNI) with 0.08Hz and 0.01Hz bounds, linear and quadratic trends removing, transformation into MIN152 space (fsl) with a 12 degrees of freedom affin transformation, (AFNI) and extraction of global, white matter and cerebrospinal fluid nuisance signals.

**Dual task experiments:** Sixteen participants (7 women and 9 men, mean age, 23, ranging from 20 to 28) were asked to perform two consecutive tasks with the instruction of providing fast and accurate responses to each of them. The first task was a visual task of comparing a given number (target T1) to a fixed reference, and, second, an auditory task of judging the pitch of an auditory tone (target T2) [24]. The two stimuli are presented with a stimulus onset asynchrony (SOA) varying from: 0, 300, 900 and 1200 ms. Subjects had to respond with a key press using right and left hands, whether the number flashed on the screen or the tone were above or below a target number or frequency, respectively. Full details and preliminary statistical analysis of this experiment have been reported elsewhere [15, 24].

Subjects performed a total of 160 trials (40 for each SOA value) with a 12 s inter-trial interval in five blocks of 384 s with a resting time of  $\sim 5$  min between blocks. In our analysis we use all scans, that is, scans coming from all SOA. Since each of the 16 subjects perform four SOA experiments, we have a total of 64 brain scans. The experiments were performed on a 3T fMRI system (Bruker). Functional images were obtained with a T2\*-weighted gradient echoplanar imaging sequence [repetition time (TR) 1.5 s; echo time 40 ms; angle 90; field of view (FOV) 192 × 256 mm; matrix 64 × 64]. The whole brain was acquired in 24 slices with a slice thickness of 5 mm. Volumes were realigned using the first volume as reference, corrected for slice acquisition timing differences, normalized to the

standard template of the Montreal Neurological Institute (MNI) using a 12 degree affine transformation, and spatially smoothed (FWHM = 6mm). High-resolution images (three-dimensional GE inversion-recovery sequence, TI = 700 mm; FOV =  $192 \times 256 \times 256$  mm; matrix =  $256 \times 128 \times 256$ ; slice thickness = 1 mm) were also acquired. We computed the phase and amplitude of the hemodynamic response of each trial as explained in M. Sigman, A. Jobert, S. Dehaene, Parsing a sequence of brain activations of psychological times using fMRI. *Neuroimage* **35**, 655-668 (2007). We note that the present data contains a standard preprocessing spatial smoothing with gaussian kernel (FWHM=6mm), which was not applied in Ref. [15]. Such smoothing produces smaller percolation thresholds as compared with those obtained in Ref. [15].

**Construction of brain networks:** In order to build brain networks in both experiments, we follow standard procedures in the literature [15, 20, 21]. We first compute the correlations  $C_{ij}$  between the BOLD signals of any pair of voxels  $i$  and  $j$  from the fMRI images. Each element of the resulting matrix has value on the range  $-1 \leq C_{ij} \leq 1$ . If one considers that each voxel represents a node from the brain network in question, it is possible to assume that the correlations  $C_{ij}$  are proportional to the probability of nodes  $i$  and  $j$  being functionally connected. Therefore, one can define a threshold  $T$ , such that if  $T < C_{ij}$  the nodes  $i$  and  $j$  are connected. We begin to add the links from higher values to lower values of  $T$ . This growing process can be compared to the bond percolation process. As we lower the value of  $T$ , different clusters of connected nodes appear, and as the threshold  $T$  approaches a critical value of  $T_c$ , multiple components merge forming a giant component.

In random networks, the size of the largest component increases rapidly and continuously through a critical phase transition at  $T_c$ , in which a single incipient cluster dominates and spans over the system [18]. Instead, since the connections in brain networks are highly correlated rather than random, the size of the largest component increases progressively with a series of sharp jumps. These jumps have been previously reported in Ref. [15]. This process reveals the multiplicity of percolation transitions: percolating networks subsequently merge in each discrete transition as  $T$  decreases further. We observe this structure in the two datasets investigated in this study: for the human resting state in Fig. 3a and for the human dual task in Fig. 3b.

For each dataset we identify the critical value of  $T$ , namely  $T_c$ , in which the two largest components merge, as one can notice in Fig. 3 in the main text. While the anatomical



projection of the largest component varied across experiments, this merging pattern at  $T_c$  was clearly observed in each participant of the two experiments analyzed here, two examples are shown in Figs. 3a-b. The transition is confirmed by the measurement of the second largest cluster which shows a peak at  $T_c$ , see Fig. 7.

For  $T$  values larger than  $T_c$  the two largest brain clusters are disconnected, forming two independent networks. Each network is internally connected by a set of strong-links, which correspond to  $k_{\text{in}}$  [15] in the notation of systems of networks. By lowering  $T$  to values smaller than  $T_c$ , the two networks connect by a set of weak-links, which correspond to  $k_{\text{out}}$  [15], i.e. the set of links connecting the two networks.

Our analysis of the structural organization of weak links connecting different clusters is performed with  $T_0 < T < T_c$ . Here,  $T_0$  is chosen in such a way that the average  $\langle k_{\text{out}} \rangle$  of outgoing degrees of the nodes on the two largest clusters is  $\langle k_{\text{out}} \rangle = 1$ . For lower values of  $T_0$ , where  $\langle k_{\text{out}} \rangle = 2$  and  $= 5$ , we found no relevant difference with the studied case of  $\langle k_{\text{out}} \rangle = 1$ .

As done in previous network experiments based on the dual task data [15] we create a mask where we keep voxels which were activated in more than 75% of the cases, i.e., in at least 48 instances out of the 64 total cases considered. The obtained number of activated voxels in the whole brain is  $N \approx 60,000$ , varying slightly for different individuals and stimuli. The ‘activated or functional map’ exhibits phases consistently falling within the expected response latency for a task-induced activation [24]. As expected for an experiment involving visual and auditory stimuli and bi-manual responses, the responsive regions included bilateral visual occipito-temporal cortices, bilateral auditory cortices, motor, premotor and cerebellar cortices, and a large-scale bilateral parieto-frontal structure. In the present analysis we follow [15] and we do not explore the differences in networks between different SOA conditions. Rather, we consider them as independent equivalent experiments, generating a total of 64 different scans, one for each condition of temporal gap and subject.

The following emergent clusters are seen in resting state: medial prefrontal cortex, posterior cingulate, and lateral temporoparietal regions, all of them part of the default mode network (DMN) typically seen in resting state data and specifically found in our NYU dataset [23].

### A. Computation of parameters $\gamma$ , $\alpha$ , $\beta$ , and $k_{\max}$

Once  $T_c$  is determined, we are able to compute the degree distribution of the brain networks. For a given brain scan we search for all connected components of strong links with  $C_{ij} > T_c$ , where  $T_c$  is the first jump in the largest connected component as seen in Fig. 3. We then calculate  $P(k_{\text{in}})$  using all brain networks for a given experiment; the results are plotted in Fig. 3. We consider all nodes with  $k_{\text{in}} \geq 1$  at  $T_c$  from all the connected clusters. As one can see in Fig. 3b, for all data sets, we found degree distributions which can be described by power laws  $P(k_{\text{in}}) \sim k_{\text{in}}^{-\gamma}$  with a given cut-off  $k_{\max}$ . For the resting state, we found  $\gamma = 2.85 \pm 0.04$  and  $k_{\max} = 133$  while for the dual task we found  $\gamma = 2.25 \pm 0.07$ ,  $k_{\max} = 139$  (see Table I). We use a statistical test based on maximum likelihood methods and bootstrap analysis to determine the distribution of degree of the networks. We follow the method of Clauset, Shalizi, Newman, SIAM Review **51**, 661 (2009) of maximum likelihood estimator for discrete variables which was already used in our previous analysis of the dual task data [15].

We fit the degree-distribution assuming a power law within a given interval. For this, we use a generalized power-law form

$$P(k; k_{\min}, k_{\max}) = \frac{k^{-\gamma}}{\zeta(\gamma, k_{\min}) - \zeta(\gamma, k_{\max})}, \quad (23)$$

where  $k_{\min}$  and  $k_{\max}$  are the boundaries of the fitting interval and the Hurwitz  $\zeta$  function is given by  $\zeta(\gamma, \alpha) = \sum_i (i + \alpha)^{-\gamma}$ . We set  $k_{\min} = 1$ .

We calculate the slopes in successive intervals by continuously increasing  $k_{\max}$ . For each one of them we calculate the maximum likelihood estimator through the numerical solution of

$$\gamma = \text{argmax} \left( -\gamma \sum_{i=1}^M \ln k_i - M \ln [\zeta(\gamma, k_{\min}) - \zeta(\gamma, k_{\max})] \right), \quad (24)$$

where  $k_i$  are all the degrees that fall within the fitting interval and  $M$  is the total number of nodes with degrees in this interval. The optimum interval was determined through the Kolmogorov-Smirnov test.

For the goodness-of-fit test, we use KS test generating 10,000 synthetic random distributions following the best-fit power law. Analogous analysis is performed to test for a possible exponential distribution to describe the data. We use KS statistics to determine the optimum fitting intervals and also the goodness-of-fit. In all the cases where the power law was

accepted we ruled out the possibility of an exponential distribution, see [15].

In order to compute the correlation of  $k_{\text{in}}$ ,  $k_{\text{out}}$  and  $k_{\text{in}}^{\text{nn}}$  we consider the following statistics for the weak links and the degrees of the external nearest neighbors of an outgoing node. This correlation is gathered from the calculation of the average in-degree,  $\langle k_{\text{in}}^{\text{nn}} \rangle$  of the external neighbors of a node with in-degree  $k_{\text{in}}$ . The strong-links are those links added to the network for  $T > T_c$ . The weak links are those added to the network for values of  $T_0 < T < T_c$  until the average out-degree reaches  $\langle k_{\text{out}} \rangle = 1$ . For statistical determination of the scaling properties of weak-links, we consider that they connect two nodes in different networks, or even nodes in the same component. To calculate the statistical scaling properties of weak links, we consider the out-weak-degree  $k_{\text{out}}$  of a node as the number of all links added for  $T_0 < T < T_c$ .

Figure 3f shows that the scenario for the correlation between  $\langle k_{\text{in}}^{\text{nn}} \rangle$  and  $k_{\text{in}}$  is consistent with Eq. (2). For the resting state experiments (Fig. 3f) there is a positive correlation between the  $k_{\text{in}}$  of outgoing nodes placed in different functional networks. For the dual-task human subjects (Fig. 3f) the correlation is also positive.

Moreover, when analyzing the relation between  $k_{\text{in}}$  and  $k_{\text{out}}$  for the same outgoing nodes, they are described by the correlations presented in Fig. 3e using power laws. Figures 3e-f depict the power-law fits using Ordinary Least Square method within a given interval of degree. We assess the goodness of fitting in each interval via the coefficient of determination  $R^2$ . We accept fittings where  $R^2 \gtrsim 0.9$ . The exponents measured are presented in Table I.

Figures 4a and b show the results we found when we apply the theory presented in Section I of this Supplementary Information on two coupled networks of degree exponent  $\gamma = 2.85$  and 2.25, respectively with the cut-off given by  $k_{\text{max}} = 133, 139$ , respectively as given by the values for human resting state and dual task. For  $\gamma = 2.25$  and  $\gamma = 2.85$ , the value associated with the data gathered from humans, the results are similar with those presented on Fig. 2 in both theoretical cases, the conditional (left panels) and redundant (right panels) interactions. The main differences between the results for  $\gamma = 2.25$  and 2.85 are the values found for  $p_c$ , where the values found for  $\gamma = 2.25$  are systematically smaller than the values found for  $\gamma = 2.85$ , going from  $p_c \approx 0.1$  to  $\approx 0.6$  for  $\gamma = 2.25$ , and from  $p_c \approx 0.1$  to  $\approx 0.8$  for  $\gamma = 2.85$ . These results can be understood from the knowledge gathered on the percolation of single networks [19]. For lower values of the degree exponent  $\gamma$  the hubs on scale-free networks become more frequent, protecting the network from breaking apart.

When comparing the two cases of Fig. 4 with the theoretical case of  $\gamma = 2.5$  (Fig. 2), one can notice that the broader the distribution (as lower the value of  $\gamma$ ), the more robust is the system of coupled networks. These general trends are consistent with the calculations of  $p_c$  for unstructured interconnected networks with one-to-one connections done in Ref. [3]. The white circles in Fig. 4 correspond to the values of  $\alpha$  and  $\beta$  measured from real data. As one can see, the experimental values are placed on the region that represents the best compromise between the predictions for optimal stability under conditional and redundant interactions.

It is also interesting to note that the extreme vulnerability predicted in Ref. [3] can be somehow mitigated by decreasing the number of one-to-one interconnections as shown in Parshani, R., Buldyrev, S. V. & Havlin, S. Interdependent networks: reducing the coupling strength leads to a change from a first to second order percolation transition. *Phys. Rev. Lett.* **105**, 048701 (2010). However, in this case, the system of networks may be rendered non-operational due to the lack of interconnections. Indeed, by connecting both networks with one-to-one outgoing links and by making these interconnections at random, there is a high probability that a hub in one network will be connected with a low degree node in the other network. These low degree nodes are highly probable to be chosen in a random attack, thus the hubs become very vulnerable due to the conditional interaction with a low degree node in the other network. This effect leads to the catastrophic cascading behavior found in [3].

Another way to protect a network in the conditional mode is to increase the number of out-going links per nodes, since the failure of a node occurs when all its inter-linked nodes have failed. Thus, by just increasing the number of interlinks from one to many out-going links emanating from a given node, larger resilience is obtained. If these links are distributed at random, then this situation corresponds to  $\alpha = \beta = 0$  in our model. However, in this random conditional case, the network may be rendered non-operational due to the random nature of the interlink connectivity. A functional real network is expected to be operating with correlations and therefore the most efficient structure when there are many correlated links connecting the networks is the one found for the brain networks investigated in the present work. In other words, assuming that a natural system like the brain functions with intrinsic correlations in inter-network connectivity, then the solution found here (large  $\alpha$  and  $\beta > 0$ ) seems to be the natural optimal structure for global stability and avoidance of

systemic catastrophic cascading effects.

Another problem of interest is the targeted attack of interdependent networks as treated in Huang, X., Gao, J., Buldyrev, S. V., Havlin, S. & Stanley, H. E. Robustness of interdependent networks under targeted attack. *Phys. Rev. E* **83**, 065101 (2011). It would be of interest to determine how the present correlations affect the targeted attack to, for instance, the highly connected nodes.

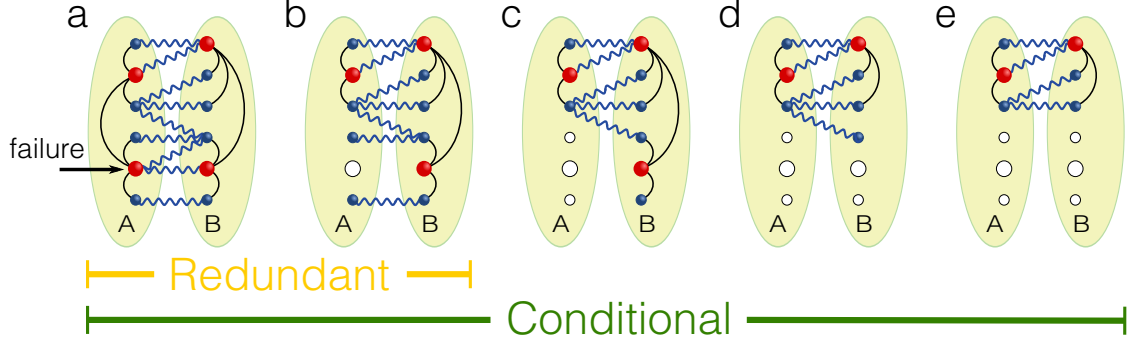


FIG. 5. Pictorial representation of the **a-e** conditional and **a-b** redundant modes of interaction. **a**, One node is removed, or fails, in network *A*, **b**, as in a regular percolation process this node is removed together with its links. In the redundant mode of interaction, the neighbors of this node are not removed, because they still maintain connection with the giant component from network *B*, but **c**, for the conditional mode of interaction the two nodes are removed, since they do not belong to the giant component of network *A*. **d**, As a consequence of the removal of the nodes in network *A* all the nodes from network *B* that lose connectivity with network *A* are also removed. **e**, Finally, the last node from network *B* is removed once it loses connectivity with the giant component of network *B*. In the end, for the conditional mode of interaction, only the mutually connected component remains.

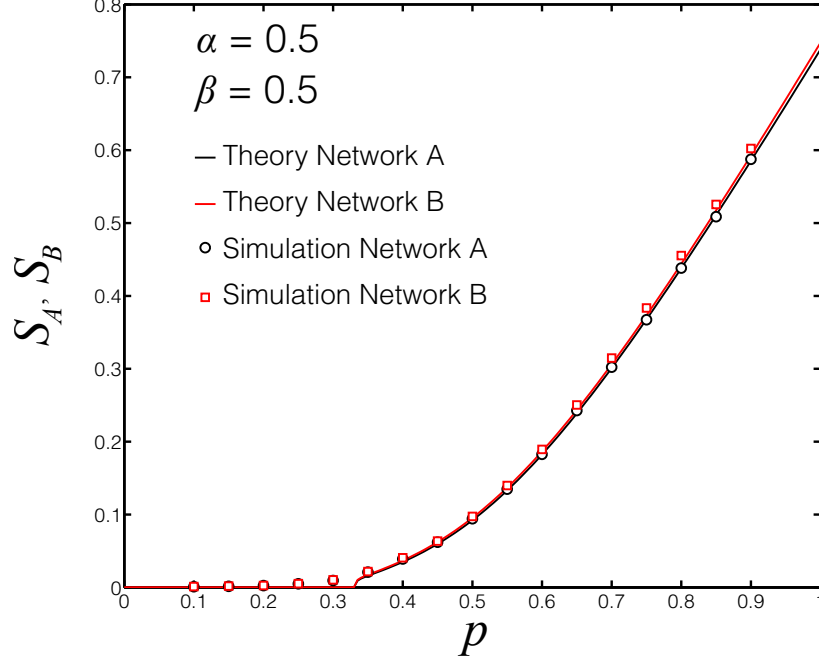


FIG. 6. Giant component of network  $A$  and  $B$  in the conditional mode of failure. We present the prediction of the theory for values of  $N_A = N_B = 1500$ ,  $\gamma = 2.5$ ,  $\alpha = 0.5$ ,  $\beta = 0.5$  and  $k_{\max} = 100$  and compare with computer simulations of the giant component obtained numerically by attacking the same network. We perform average over 100 different realizations. We attack a fraction  $1 - p$  of both networks and calculate the fraction of nodes belonging to the corresponding giant components. The results show a very good agreement between theory and simulations.

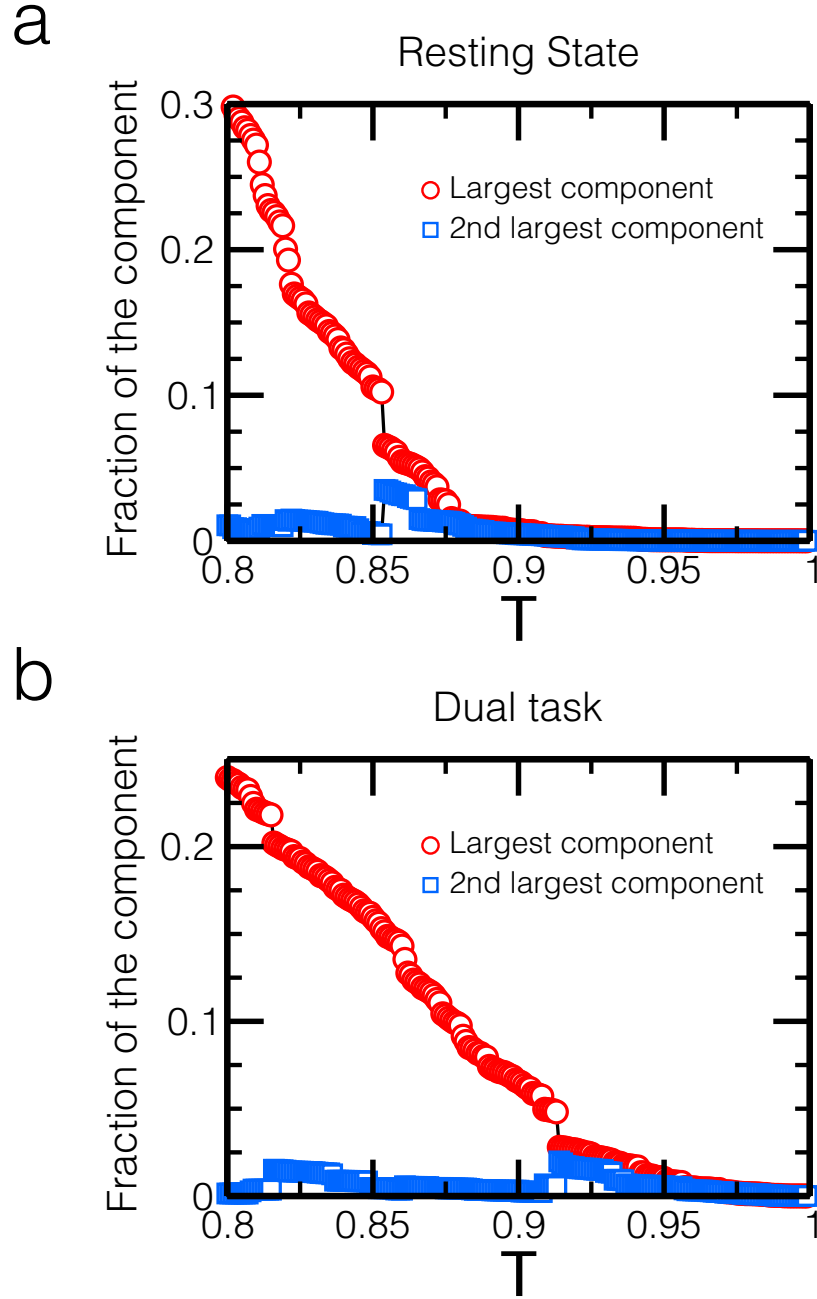


FIG. 7. First and second largest component in the brain networks corresponding to resting state and dual task. The largest component shows a jump while the second largest component shows a peak, indicating a percolation transition at  $T_c$ . **a**, Resting state. **b**, Dual task.